

Chapter 15

Pressure dependence on the magnetic properties of titanomagnetite using the reversible susceptibility method

Stuart A. Gilder and Maxime LeGoff

Abstract

This chapter describes an alternating current susceptibility system, constructed for the diamond anvil cell, that facilitates the acquisition of reversible susceptibility hysteresis loops as a function of pressure. The technique is particularly adapted to studying the effects of stress on the magnetic properties of multidomain grains because the contribution to the full (differential) susceptibility is equivalent to reversible susceptibility for such grain sizes. Here, we apply the method to synthetic multidomain grains in the titanomagnetite solid-solution series with phases containing 20, 40, and 60% Ti, and compare the results with those previously obtained from pure (0% Ti) magnetite. We show that initial susceptibility (X_{max}) and saturation moment (M_s) decrease as a function of increasing pressure and Ti concentration. The decrease is ascribed to the rotation of domains into alignment perpendicular with the maximum stress direction, conversion of a part of the reversible susceptibility into irreversible susceptibility, and an increase in the demagnetization energy via the creation of lamellar domains as well as the disappearance of closure domains. We define a constant called the median destructive stress, which is the pressure needed to remove one-half of the original susceptibility, and we show that this value is proportional to the inverse of the magnetostriction constant (λ_s), consistent with established theory. Another suite of experiments is designed to estimate the amount of reversible susceptibility that is converted into irreversible susceptibility and to determine the effect that the conversion has on $M_s(P)$. Changes in X_{max} and M_s occur fairly systematically across titanomagnetite species, with M_s/X_{max} initially increasing with pressure, before reaching a constant value where M_s becomes proportional to $4/3 X_{max}$. Such behavior is attributed to systematic variations in domain wall motion in relation to stress and λ_s .

1. Introduction

Although the influence of temperature on magnetic remanence has long been a subject of research, much less is known about how pressure modifies the magnetic properties of materials. Advances in this field have been largely inhibited by experimental constraints. Early work employed large piston presses situated in proximity to astatic or flux gate magnetometers (e.g. Pozzi, 1973). Detection limits of these systems required large samples because of their higher magnetic intensities; however, the large sample sizes prevented applied pressures from exceeding a few kilobars, e.g. a few tenths of a gigapascal. Moreover, the early experimental apparatuses could only measure magnetizations along a single axis, and the applied stresses were commonly non-hydrostatic. As high-pressure investigation advanced, it became apparent that magnetic properties were

sensitive to the applied stress direction and the type of imposed stress (Kean et al., 1976; Hamano, 1983; Kapicka, 1990; Valeev and Absalyamov, 2000). For stress demagnetization (i.e. stress applied in the absence of an applied magnetic field), magnetization intensity decreases faster parallel to the maximum stress direction rather than perpendicular to it. When pressure is applied in the presence of a magnetic field, both magnetic susceptibility and magnetization increase in intensity perpendicular to the maximum stress direction and decrease parallel to the maximum stress direction.

Other research has focused on how stress influences the magnetic moment at the atomic level. For example, the Mössbauer resonance technique yields important information about the existence and type of magnetic network in materials and about how those networks respond to applied stresses and magnetic fields. Although Mössbauer resonance has made important advances in understanding high-pressure phase transitions, the method does not quantify magnetic parameters such as intensity and direction of the moment, nor their stress dependencies, which are essential parameters in the Earth and planetary sciences.

More recently, BeCu and NiCrAl alloys and ceramics have been exploited in the construction of diamond or sapphire anvil cells that can achieve pressures well into the gigapascal range (e.g. Yamamoto et al., 1991; Eremets et al., 1995). The slightly magnetic nature and relatively high strength of the alloys has opened new avenues of high-pressure studies on magnetism (Tozer, 1993; Timofeev et al., 1999). Using this new technology, and adapting a technique that was originally used in superconductivity research, we developed a system that measures reversible susceptibility hysteresis loops at high pressures, which allows one to quantify the stress dependency on magnetic hysteresis parameters. Other workers have used the reversible susceptibility technique to measure tensor hysteresis loops in pipe steel (Mao and Atherton, 2000), temperature dependence on magnetic moment (Ishizuka et al., 1995) and magnetic phase transitions in invar alloy (Endo et al., 1999). It is the ability to measure hysteresis loops and to derive the associated magnetic hysteresis parameters that distinguishes our method from others using the reversible susceptibility technique. In this chapter, we describe this new method and apply it to titanomagnetite, which is an important carrier of magnetic remanence in rocks.

2. Sensor design and cell description

The measuring system we used was described in Kim et al. (1994) (see also Gilder et al., 2002; Struzhkin et al., 2002). The principle is based on the Lenz/Faraday law of electromotive force ($\text{emf} = -d\phi/dt$, where ϕ is the magnetic flux passing through an electric circuit. With a coil of surface S immersed in a variable field B , the $\text{emf} = -S(dB/dt)$, and with a magnetic moment M placed near a coil system, the $\text{emf} = -S(d(MG)/dt)$, with $G = B/i$ being related to the coil geometry. Our system employed two unequal pick-up coils of 351 (detection coil) and 195 turns (compensation coil) with diameters of 3 and 4.5 mm, respectively, that were wound in opposition around a diamond (culet diameter = 370 μm), resulting in a virtually null magnetic surface (Fig. 1). This configuration has the advantage that varying magnetic field fluxes passing through both coils provoke no induction, whereas, if one coil senses a different flux than the other, the system becomes unbalanced and a voltage is generated. It follows that

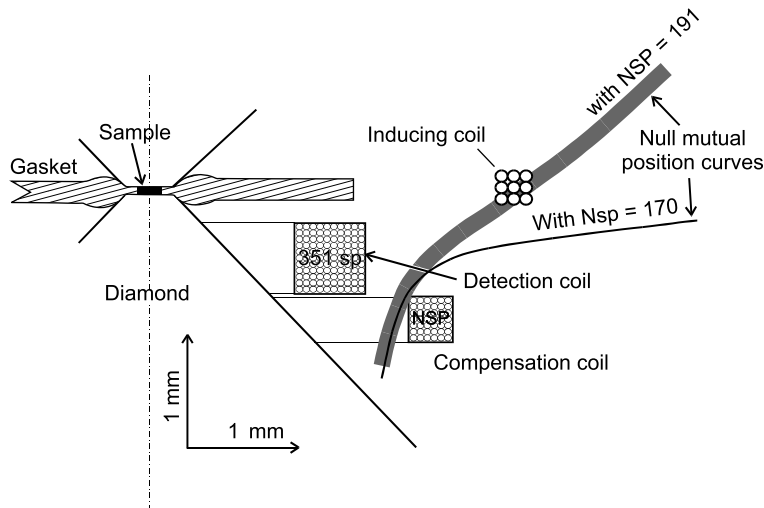


Figure 1. Diagram of the coaxial AC susceptibility measuring system. The thick gray and thin black lines satisfy the null mutual position of the induction coil when the compensation coil has 191 and 170 turns (Nsp) of wire, respectively. The inducing coil is glued to a support fixed to the compensation and detection coils.

the greater the number of turns of wire, and the closer the detection coil is to the magnetic source, the greater the sensitivity.

Fixed above the pick-up coils is an inducing coil, mounted in null mutual inductance, which produced a peak alternating current (AC) field of 2×10^{-4} T over the sample region. Achieving an exact surface equilibrium of both pick-up coils is not too critical when using a digital signal processor (DSP) lock-in amplifier working at frequencies higher than 10 kHz, in a magnetically quiet environment. On the contrary, the position of the induction coil requires that both pick-up coils sense as close to the same flux as possible because thermal effects on the coils are difficult to compensate with electronic circuitry. Thus, it is preferable to minimize the near null mutual induction before mounting the inducing coil. In a co-axial configuration for all three coils, which we employed (Fig. 1), the radius of the inducing coil and its distance from the detection coil have several solutions. Figure 1 shows the range of possibilities where to place the inducing coil, with the thick line representing the null mutual solution. We designed the system so that the detection coil has the smallest possible radius and sits as close as possible to the sample, and that the inducing coil lies within the plane of the sample (Fig. 1). The inducing coil must be large enough to allow a gasket to be placed within its confines, while the detection coil must be positioned low enough on the diamond so that when the diamond indents into the gasket, it does not press on the coils. The final sensitivity, given the radius and number of turns, is about 10^{-9} A m²/μV.

We originally constructed the coils following the description of Kim et al. (1994) by machining a lucite form, then winding a 25 μm-diameter copper wire, insulated with 5 μm-thick isolation (total diameter = 35 μm), around it. We fixed the windings with a non-magnetic, water-soluble glue (Elmer's Glue-All) so they would not unbind when dissolving the lucite in methylene chloride. Although successful, we improved the

manufacturing of subsequent coils by coating the diamond in epoxy resin (Araldite), then machining the form directly on the diamond. This eliminates the need to dissolve the form, which often causes some spires to unravel, and then fix the coils to the diamond, which risks cutting the thin wire. One encounters the greatest difficulty with the new method when laying the first turn, as it breaks easily due to the high number of windings. To avoid this problem, we cut a small channel in the form, placed the wire in it, and blanketed the wire in a coat of glue. The null mutual position of the inducing coil was found by observing the induced signal from the pick-up coils with an oscilloscope. Araldite was used to fix the inducing coil because its volume changes negligibly when drying.

A Stanford Research Systems SRS830 lock-in amplifier measured the output of the sensing coil and a homemade current supply was built for the inducing coil (Fig. 2). Because both in-phase and quadrature components are registered, one needs to verify which component corresponds to magnetic susceptibility. This is done by introducing a piece of pure magnetite in the measuring region then adjusting the phase on the SRS830 accordingly. The other component thus corresponds to electrical conductivity and to the non-linearity of the minor hysteresis loop (Mullins and Tite, 1973); however, the phase is set so that the system is nearly completely tuned to recover only the in-phase (susceptibility) signal while neglecting the quadrature (conductivity) signal. It is important to note that this system could be developed in the opposite sense, i.e. to measure the electrical conductivity of material under pressure. Although one attempts to fix the induction coil as close to the null position as possible, there always exists a non-perfectly null component, which can be compensated by electronic circuitry. This is done

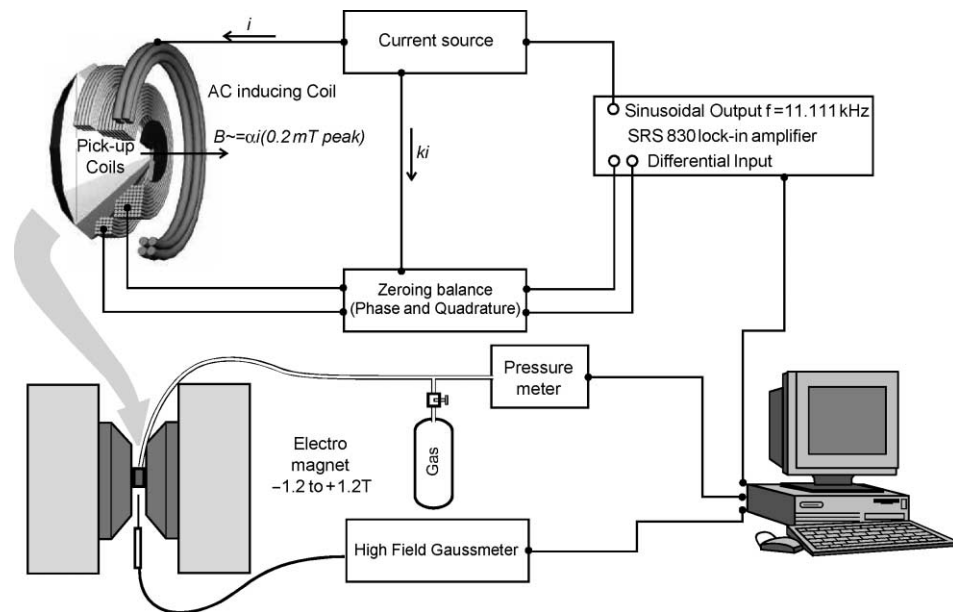


Figure 2. Cartoon of the experimental set-up. The coils are housed in a membrane-type BeCu diamond anvil cell that is attached to a helium gas tank via a capillary tube. The cell is placed in the electromagnet with the axis of the AC field parallel to the DC field generated by the electromagnet. The diameter of the pole pieces is 15 cm with a gap of 5 cm. See text for more details.

by deflecting a small part of the in-phase and quadrature currents to the voltmeter via trimming potentiometers (Fig. 2). By adjusting the potentiometers, one obtains a nearly perfect null signal.

Noise at the entrance of the system is <10 nV (about 10^{-11} A m²) with integration times of 300 ms at an operating frequency of 11.111 kHz. Given a magnetite volume of 1.5×10^{-2} mm³ in a 200- μ T AC field, the induced moment corresponds to 10^{-8} – 10^{-9} A m², well above the noise level. Analytical results were verified to be proportional over frequencies from 1 to 12 kHz with greater sensitivity at higher frequencies. Both diamonds are glued to sapphire cylinders, which are in turn housed within a membrane-type DAC made entirely of BeCu alloy (Chervin et al., 1995), which is in turn placed in the confines of an electromagnet with a 5 cm gap between pole pieces, each with an effective diameter of 15 cm (Fig. 2). The measuring axis and the high field direction are parallel. Pressure is controlled remotely by compressed helium, which avoids having to displace the cell during the course of an experiment.

3. Details of the AC susceptibility method

When exposed to an external field (H), a ferromagnetic substance acquires a magnetic moment (M), which varies nonlinearly until saturation (Fig. 3a). The value of M depends on whether H is increasing or decreasing: the curve $M(H)$ defines a hysteresis loop whose derivative dM/dH is the differential susceptibility (X_{diff}) (Fig. 3b). When a small AC field is added, M does not follow the full hysteresis loop, but instead defines a minor loop, within the interior of the hysteresis loop, whose slope ($\Delta M/\Delta H$) is less than dM/dH and is called reversible susceptibility (X_{rev}) (Fig. 3a) (Bertotti, 1998). In other words, X_{diff} changes as a function of H whose integral defines a hysteresis loop ($M(H) = C + \int_{H_0}^H X_{\text{diff}}(H)dH$) that has both irreversible and reversible parts ($X_{\text{diff}} = X_{\text{irr}} + X_{\text{rev}}$). Because our technique uses an AC field to measure susceptibility, only the reversible part is recovered. Thus the integral of $X_{\text{rev}}(H)dH$ may not fully approach the full (differential) hysteresis loop and may underestimate its associated parameters of saturation magnetization (M_s), remanent saturation magnetization (M_{rs}) and coercivity (H_c).

Reversible contributions are different in multi- and single-domain grains (Dunlop and Özdemir, 1997). Hysteresis in multidomain magnetite is controlled by domain wall displacement, where domains whose magnetizations are favorably oriented with the applied field direction grow at the expense of neighboring domains. In contrast, hysteresis of single domain grains is produced by irreversible jumps of the magnetization vector from one easy magnetic axis to another that is oriented closer in line with the applied field direction. Reversibility occurs only before and after a jump, by deviation of the spontaneous magnetization around the easy axis oriented in the field direction. Thus $X_{\text{rev}} \Rightarrow X_{\text{diff}}$ in multidomain magnetite (where H_c and M_{rs} are small) due to the reversibility of wall displacements, while X_{rev} contributes much less to X_{diff} in single domain magnetite.

Figures 4 and 5 illustrate the differences in X_{rev} between multi- and single domain magnetite. Figure 4a shows the measured hysteresis loop $M(H)$ of pure multidomain magnetite, and the derivative of that loop ($X_{\text{diff}}(H)dH$) is plotted in Figure 4b. For comparison, Figure 4c shows the measured AC susceptibility loop ($X_{\text{rev}}(H)$) of a different

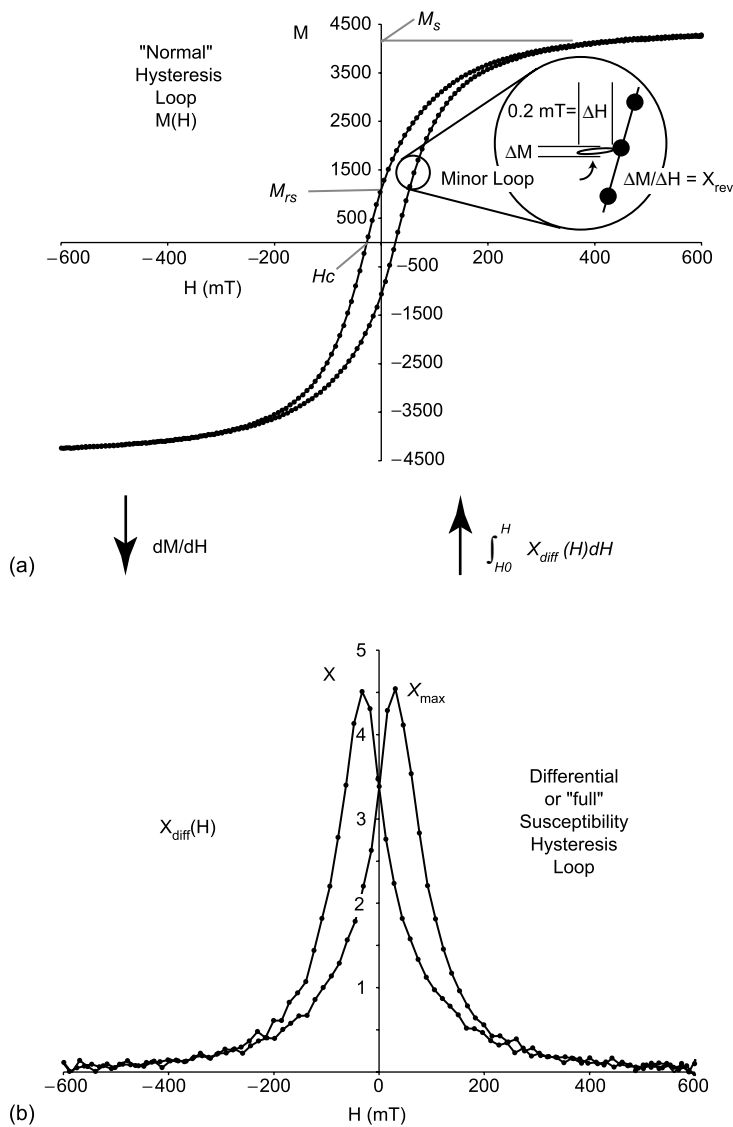


Figure 3. Explanation of the AC susceptibility method. (a) A full hysteresis loop $[M(H)]$ of single domain magnetite (chiton teeth). The sinusoidal AC field forms minor loops within the interior of the full hysteresis loop. The width of the loop (ΔH) is the amplitude of the AC field (0.2 mT in this case) while the height of the loop (ΔM) is the amount of magnetization gained or lost under the 0.2 mT AC field. Reversible susceptibility (X_{rev}) equals $\Delta M/\Delta H$. (b) The derivative of the full hysteresis loop (dM/dH) is the differential, or full, susceptibility hysteresis loop $[X_{diff}(H)]$. Put another way, if one measured $X_{diff}(H)$, then took its integral, it would yield $M(H)$.

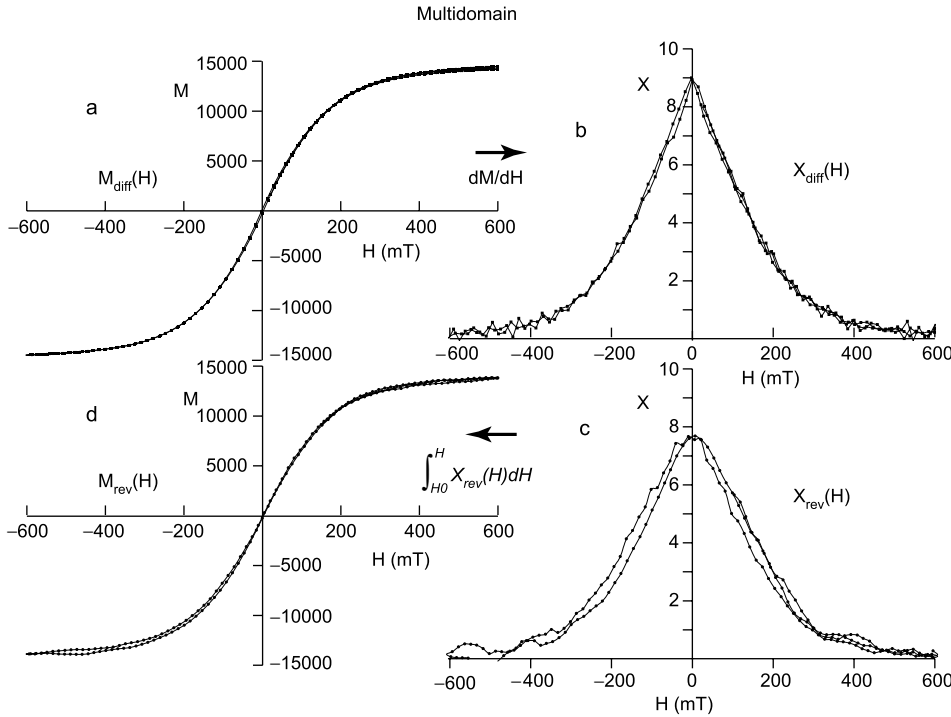


Figure 4. Comparison of the differential (full) and reversible hysteresis loops for the same sample of multidomain magnetite (TM0, magnetite extracted from the Mt Givens [California] pluton). (a) The measured differential [$M(H)$ or $M_{diff}(H)$] hysteresis loop and its derivative (b) that yields $X_{diff}(H)$. (c) The measured reversible susceptibility loop $X_{rev}(H)$ and its integral (d) that yields $M_{rev}(H)$. Note the resemblance between $M_{diff}(H)$ and $M_{rev}(H)$ ($M_s \approx 12,500$ [arbitrary units] and $H_c < 2$ mT in both cases) and between $X_{diff}(H)$ and $X_{rev}(H)$.

multidomain magnetite sample and its integral ($\int_{H_0}^H X_{rev}(H)dH$) is plotted in Figure 4d. One observes a good correlation between X_{rev} and X_{diff} and between $M_{rev}(H)$ and $M_{diff}(H)$. We then performed the same exercise for single domain magnetite (Fig. 5a to d), where one notes a much less than ideal fit between X_{rev} and X_{diff} and between $M_{rev}(H)$ and $M_{diff}(H)$.

4. Titanomagnetite

Titanomagnetite ($Fe_{3-x}Ti_xO_4$) [also written $xFe_2TiO_4(1-x)Fe_3O_4$] forms a complete solid solution series between end members of magnetite (Fe_3O_4) and ulvöspinel (Fe_2TiO_4). They are cubic minerals with inverse spinel structures that commonly carry the magnetic remanence of rocks; i.e. TM60 ($x = 0.6$) is the dominant magnetic mineral in rapidly quenched submarine basaltic lavas. Details concerning their structural and magnetic properties can be found in Syono (1965), O'Reilly (1984), Lindsley (1991).

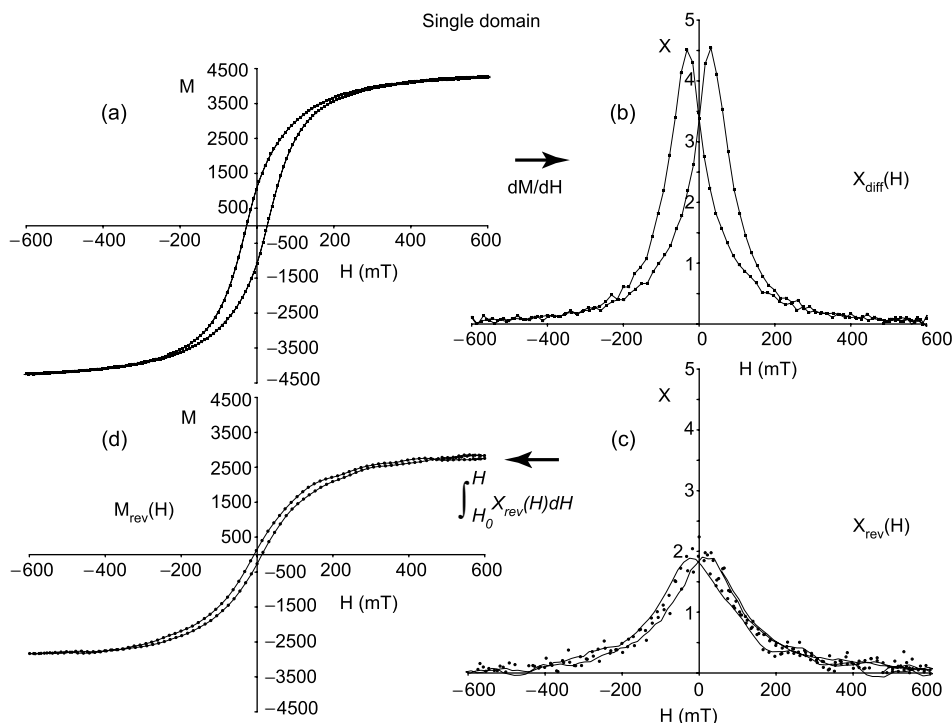


Figure 5. Comparison of the differential (full) and reversible hysteresis loops for the same sample of single domain magnetite (chiton teeth). (a) The measured differential [$M(H)$ or $M_{diff}(H)$] hysteresis loop and its derivative (b) that yields $X_{diff}(H)$. (c) The measured reversible susceptibility loop $X_{rev}(H)$ and its integral (d) that yields $M_{rev}(H)$. Note the differences between $M_{diff}(H)$ and $M_{rev}(H)$ and between $X_{diff}(H)$ and $X_{rev}(H)$. $M_{s,diff}$ and $H_{c,diff} \approx 3900$ (arbitrary units) and 27 mT; $M_{s,rev}$ and $H_{c,rev} \approx 2800$ (arbitrary units) and 11 mT.

The samples in our experiments were single titanomagnetite crystals synthesized by B.J. Wanamaker using the floating zone technique (Wanamaker and Moskowitz, 1994). Optical, Laue back-reflection and scanning electron microscopy, electron microprobe, and thermomagnetic analyses indicate that the TM60 sample is a single crystal, single phase, and chemically homogeneous except for a 3% gradient in Ti concentration over a 4 cm length of the crystal. We verified the Ti concentration and homogeneity of the samples via our own thermomagnetic analyses using an AGICO CS-3 furnace linked to a KLY-3 Kappabridge susceptibility meter (Fig. 6). Curie temperatures on heating correspond to titanium concentrations of TM19, TM39, and TM60 (Akimoto, 1962), which, given the uncertainties, are close to the intended values of $Fe_{2.8}Ti_{0.2}O_4$ (TM20), $Fe_{2.6}Ti_{0.4}O_4$ (TM40), and $Fe_{2.4}Ti_{0.6}O_4$ (TM60). Although the TM60 sample is relatively pure, TM40 and TM20 exhibit evidence for inhomogeneous or incomplete Ti diffusion during synthesis resulting in multiphase spinels. TM20 has a phase with a Curie point at 523°C (TM11) while TM40 possesses two phases with Curie points at 393°C (TM31) and 485°C (TM18). Unlike the Curie points of the major phases, those of the minor

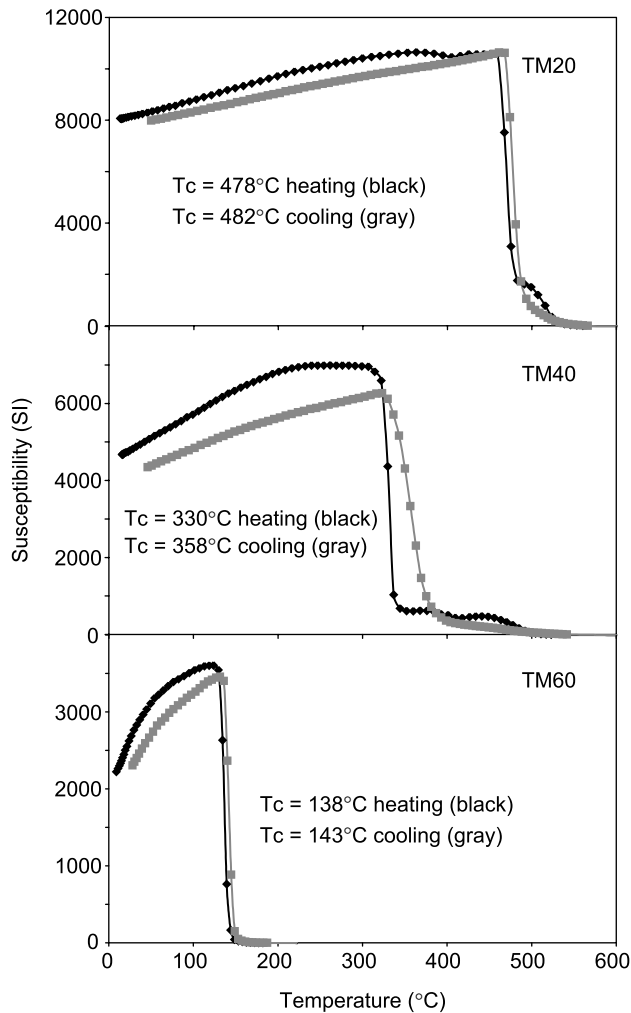


Figure 6. Curie point experiments of the three TM species (determined using an AGICO CS-3 instrument). Heating curves are in black and cooling curves are in gray. Curie temperatures are listed for each TM species. Susceptibilities have not been normalized by volume or mass.

phases are spread out over a wide temperature range, indicating a spectrum of Ti contents and related phases. However, the impurities are minor with respect to the main constituents and should not significantly influence the results. Heating stabilizes the TM20 and TM40 phases, with Curie points on cooling corresponding to TM18 and TM36. The heated material for TM20 was used in our experiments. Hysteresis experiments of the three phases reveal their multidomain nature, with imperceptible bulk coercivities and remanent saturation moments (Fig. 7), making them ideally suited for the reversible susceptibility method.

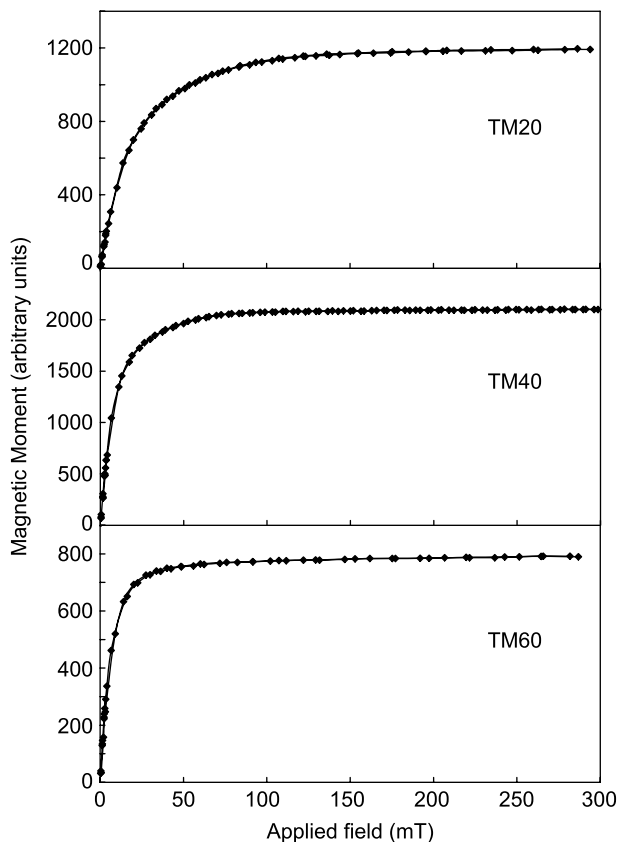


Figure 7. Hysteresis loops for each of the three TM species used in this study – only one half of the loop is shown for better observation. Moments have not been normalized by volume or mass. H_c in all cases is < 2 mT.

5. Experimental procedures and results

Experimental procedures were described in Gilder et al. (2002) and are repeated briefly here. An empty gasket was loaded in the cell, the cell was placed into the electromagnet, and the gasket was slightly compressed. Reversible susceptibility of the gasket was measured while making at least three complete cycles through applied fields of ± 1.2 T to obtain $X(H)$. After correcting for thermal drift, we stacked the curves corresponding to the three cycles and calculated the average X at each H (Fig. 8a). The cell was then removed from the electromagnet, a sample was loaded in the empty gasket, the cell was put back into the electromagnet, then $X(H)$ of the sample + gasket was measured using the same procedure previously applied to the gasket alone (Fig. 8b). The $X(H)$ of the gasket was subtracted from $X(H)$ of the sample + gasket to obtain $X(H)$ of the sample (Fig. 8b). Pressure was increased, $X(H)$ of the sample + gasket was measured at the new pressure, the $X(H)$ of the gasket was subtracted, etc. $X(H)$ of the gasket varies negligibly as a

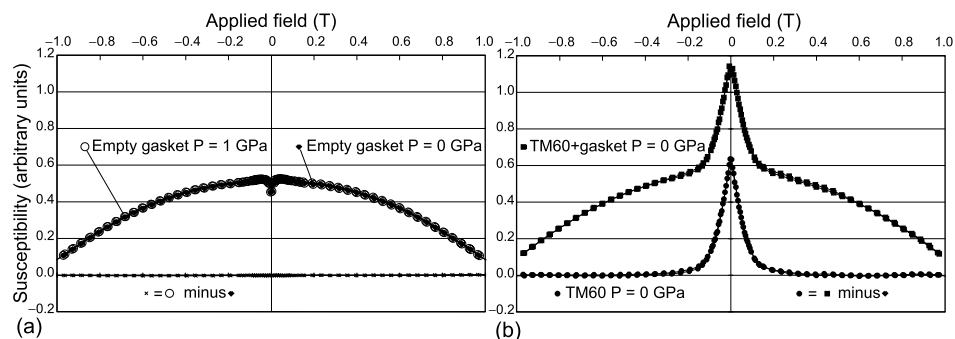


Figure 8. (a) Reversible susceptibility versus applied field of an empty gasket at high pressure (about 1 GPa) (open circles) and at ambient pressure (small solid diamonds). The difference between the two curves is negligible (small x's). (b) Reversible susceptibility versus applied field of the TM60 sample plus the gasket at $P = 0$ GPa (solid squares) and when subtracting the signal from the gasket (open circles or small solid diamonds from [a]) yielding TM60 at $P = 0$ (solid circles).

function of pressure, as seen by comparing $X(H)$ for the same gasket at $P \approx 1$ GPa and $P = 0$ GPa and their difference (Fig. 8a).

Samples consist of several tens of TM fragments, with an average size of about $20 \mu\text{m}$ /fragment, saturated in silica gel, the latter serving as a pressure medium. Although the exact amount of TM introduced in the gasket is unknown, the relative proportion of sample:gel is similar for each TM species and fairly constant across species. Knowing the precise mass of the material, by weighing beforehand, is difficult because some TM grains stay on top of the gasket during loading, then must be carefully removed to assure that no stray grains remain. We have not found a simple way to recover and then weigh those stray grains, yet this part of the procedure can be eventually improved. By filling the $\sim 150 \mu\text{m}$ -diameter hole (made by electrolysis) in the $\sim 100 \mu\text{m}$ -thick gasket to capacity, sample volumes should be similar and thus comparable.

Pressure was calibrated with ruby fluorescence (Adams et al., 1976; Chervin et al., 2001) by mimicking the pressure path of each experiment three to eight times, using the same gasket material and geometry and similar ruby:silica gel ratios as the TM:silica gel ratios (Fig. 9). Distinct $R1$ and $R2$ peaks in the spectra suggest dominantly hydrostatic pressure conditions were maintained in the cell. At 3 GPa, pressure measured on a ruby near the edge of the gasket hole is $\sim 10\%$ less than the pressure on a ruby at the center. Standard deviations are less than 0.2 GPa except at the highest pressures achieved in the TM20 experiments where they reach 0.3 GPa. While we used the mean value of the measurements, one can see in Figure 9 that pressure can vary by 0.5 GPa between two independent runs. Thus the greatest source of uncertainty in our experiments is not the relative pressure in an experiment but rather when comparing absolute pressures from one experiment to the next. Reducing this uncertainty is difficult because already the gaskets are uniform and the center of the hole can be routinely placed in the center of the diamond. Conversely, one cannot extract the cell from the electromagnet to make a pressure measurement during the course of an experiment so we see no way around the calibration method.

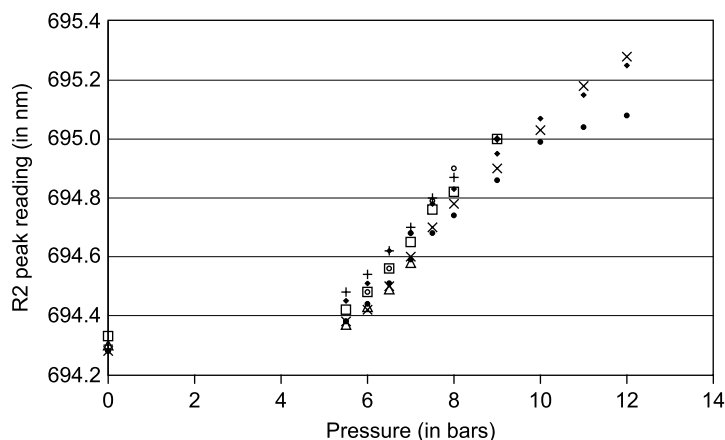


Figure 9. Pressure calibration of a BeCu gasket filled with ruby and silica gel following the experimental procedures of the type-one experiments. Each symbol represents an independent calibration. Pressure in bars is the pressure of helium gas applied to the membrane of the diamond cell (accurate to one-tenth of a bar). The R2 peak (in nanometers) is determined via ruby fluorescence then translated into pressure (Adams et al., 1976; Chervin et al., 2001).

We performed two separate experiments on each titanomagnetite phase. The first was to sequentially increase pressure until $\sim 95\%$ of the original signal was lost, then sequentially decrease pressure back to ambient conditions. The second was to compress to a pressure ($P = P1$), make a measurement, fully decompress ($P = 0$), make a measurement, raise the pressure above the previous value ($P = P2$), make a measurement, fully decompress ($P = 0$), etc. Reversible susceptibility hysteresis curves and their integrals for the type-one experiments are shown in Figure 10.

Because the samples are purely multidomain, two useful parameters are obtained from the experiments: the measured maximum reversible susceptibility (X_{\max}) and the calculated saturation moment (M_s). Both are listed in Table 1 for each pressure step. M_{rs} and H_c are too small to be accurately determined at any pressure. The fact that X_{\max} occurs at zero applied field (Figs. 4 and 10) and is measured using a 0.2 mT AC field, X_{\max} should represent the initial susceptibility of the material. Fig. 11a and b plot X_{\max} and M_s as a function of pressure for the type-one experiments for the three TM species together with the TM0 data from Gilder et al. (2002); the same data, normalized by the starting, pre-compressed values, are shown in Fig. 11c and d. One quickly notes the pressure sensitivity as a function of Ti concentration, with X_{\max} and M_s decaying faster as a function of pressure as Ti increases.

6. Discussion

So what controls the decrease in X_{\max} and M_s ? For X_{\max} , the response appears to lie in the change in domain structure. Bogdanov and Vlasov (1966) observed that, for pure magnetite, the number of domains increases as a function of stress, noting that the change in domain structure varies according to the crystallographic axis and the applied

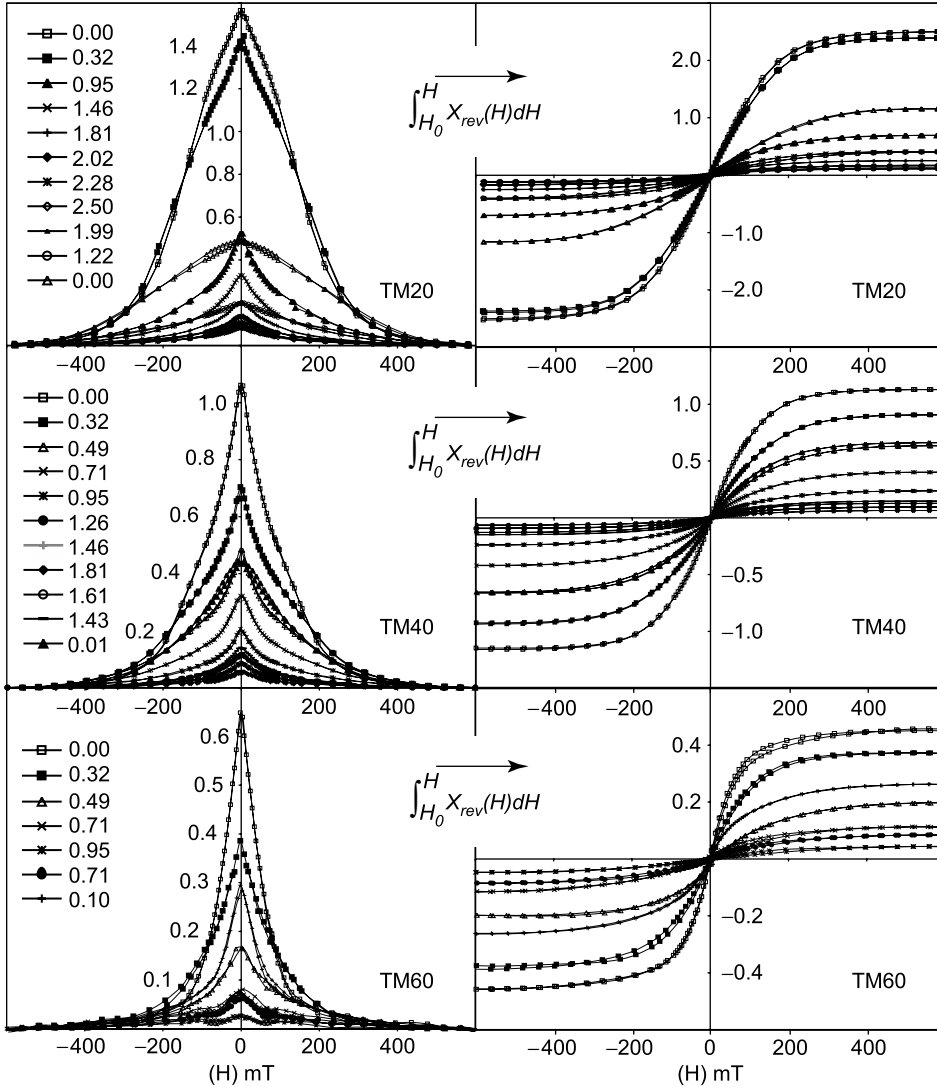


Figure 10. Measured $X_{rev}(H)$ loops for each of the TM species for the type-one experiments (left) and the integrals for each loop [$M_{rev}(H)$] (right). Pressure shown on left is in GPa, with the experiment progressing from top to bottom.

stress direction. Because the demagnetization factor (N) increases as the number of lamellar domains increases (Dunlop and Özdemir, 1997, p. 111; Dunlop, 1983) and because X varies as $1/N$ in multidomain magnetite (Néel, 1955; O'Reilly, 1984, p. 75), the measured decrease in X_{max} can be at least partly attributed to an increase in N . Moreover, Bogdanov and Vlasov (1966) found that closure domains disappear with increasing stress, which will increase the surface pole density and the magnetostatic energy of the grain (Özdemir et al., 1995), which will in turn lead to higher N .

Table 1. Reversible susceptibility parameters measured as a function of pressure.

TM20 (1)			TM20 (2)			TM40 (1)			TM40 (2)			TM60 (1)		TM60 (2)			
<i>P</i> (GPa)	Ms/1000	X_{\max}															
0.00	2.5050	1.5660	0.00	1.5600	1.1870	0.00	1.1290	1.0610	0.00	0.9070	0.7370	0.00	0.4570	0.6490	0.00	0.5640	0.9180
0.32	2.3910	1.4460	0.32	1.5300	1.0880	0.32	0.9060	0.7030	0.32	0.8440	0.6640	0.32	0.3740	0.3860	0.29	0.4410	0.5690
0.95	0.6960	0.5230	0.49	1.4750	0.8110	0.49	0.6340	0.4830	0.49	0.7930	0.6210	0.49	0.1994	0.1664	0.32	0.4350	0.4140
1.46	0.4130	0.3290	0.00	1.5260	1.1470	0.71	0.4020	0.3220	0.00	0.9230	0.8000	0.71	0.1131	0.0806	0.00	0.5360	0.7830
1.81	0.2529	0.2029	0.71	1.1360	0.5900	0.95	0.2364	0.2056	0.71	0.7010	0.5740	0.95	0.0463	0.0275	0.49	0.3210	0.2784
2.02	0.1645	0.1376	0.00	1.5220	1.0830	1.26	0.1279	0.1151	0.00	0.9070	0.7830	0.71	0.0854	0.0719	0.00	0.5100	0.6970
2.28	0.1244	0.1011	0.95	0.7540	0.4110	1.46	0.0932	0.0849	0.95	0.5990	0.5310	0.10	0.2627	0.2945	0.71	0.2490	0.2106
2.50	0.1103	0.0821	0.00	1.4810	1.0150	1.81	0.0646	0.0547	0.00	0.8760	0.7390				0.00	0.4660	0.5500
1.99	0.1738	0.1154	1.26	0.5000	0.2892	1.61	0.0935	0.0857	1.26	0.3130	0.2716				0.95	0.2069	0.1610
1.22	0.4040	0.1980	0.00	1.4160	0.9130	1.43	0.1475	0.1409	0.00	0.8260	0.6730				0.00	0.4750	0.6370
0.00	1.1580	0.4880	1.46	0.3590	0.2413	0.01	0.6600	0.4410	1.46	0.1518	0.1428				1.26	0.1986	0.1475
			0.00	1.3170	0.8030				0.00	0.7430	0.5960				0.00	0.4800	0.6190
			1.81	0.2334	0.2010				1.81	0.0588	0.0693						
			0.00	1.1620	0.6640				0.00	0.4950	0.3890						
			2.15	0.1200	0.0993												
			0.00	0.9310	0.4660												
			2.50	0.0884	0.0756												
			0.00	0.7690	0.3650												

(1) and (2) refer to type-one and two experiments, respectively. Experiments progress from top to bottom.

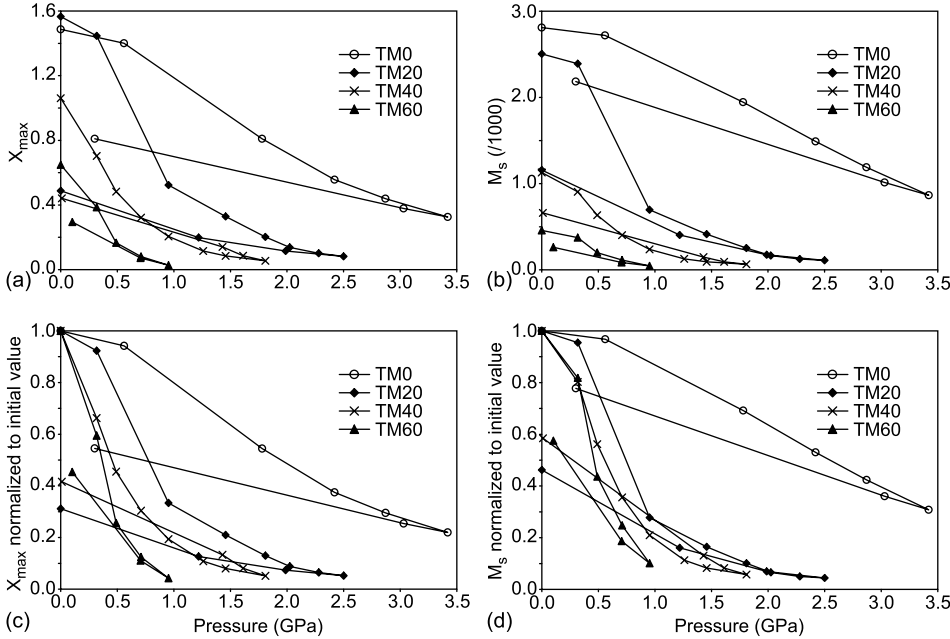


Figure 11. (a) X_{\max} and (b) M_s (multiplied by 1/1000) measured at each pressure in the type-one experiments. (c) and (d) are the same data normalized by the initial (starting) X_{\max} and M_s values, respectively. Data for TM0 were reported in Gilder et al. (2002).

Soffel et al. (1982) observed that titanomagnetites with higher ulvöspinel concentrations have curved domain walls and fewer closure domains. Thus, the decrease in $X_{\max}(P)$ is partially related to the creation of new lamellar domains and the disappearance of closure domains.

The change in domain state results from an increase in strain, due to a rise in the strain anisotropy energy (E_{anis}), where E_{anis} is expressed as $-(3/2)\lambda_s\sigma\cos^2\theta$, with λ_s being the net magnetostriction constant, σ , the applied stress, and θ , the angle between the magnetization vector of the grain relative to the applied stress direction (Kittel, 1949; Shive and Butler, 1969; Hodych, 1976; O'Reilly, 1984, p. 50). Although this parameter assumes a uniaxial stress, yet the stresses in our experiments are dominantly hydrostatic, the fact that λ_s and the compressibility of TM are anisotropic should lead to a non-null θ . This means that pressure acts to augment E_{anis} , and thus N . The reason for TM species with higher Ti to be more pressure sensitive, e.g. lose X_{\max} faster, should therefore be related to λ_s . In other words, λ_s should vary with N , and X_{\max} should be proportional to $1/\lambda_s$. Indeed, magnetostriction constants do rise as a function of titanium concentration, being 2.9, 5.0, 5.9, 8.4, 8.9 and $12.3 (\times 10^{-5})$ for TM values of 0, 4, 10, 18, 31, and 56, respectively (Syono, 1965). This implies that, not only is X_{\max} related to the spontaneous moment (decreasing effective magnetization with increasing Ti), but for multidomain grains, X_{\max} also depends on λ_s , which is consistent with theory (Kern, 1961).

As TM species become enriched in Ti, so too should they become more pressure sensitive. In order to verify this, we defined a parameter called the median destructive

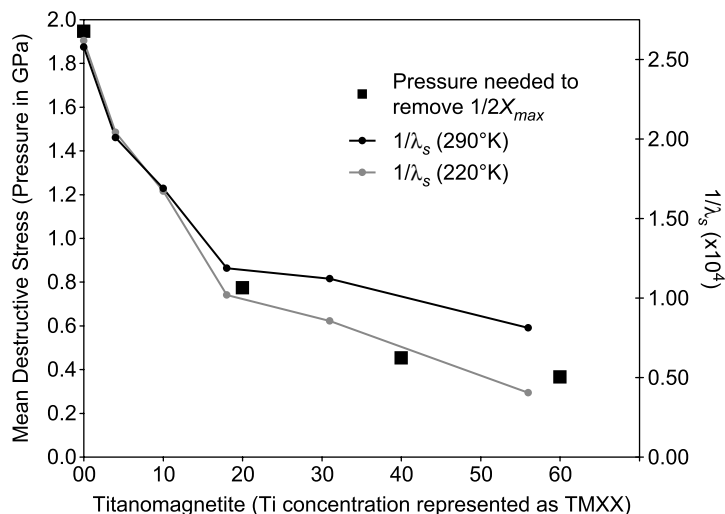


Figure 12. MDS, which is the pressure needed to reduce X_{max} to one-half of its initial value, plotted as a function of titanium concentration. Also plotted is the inverse of the magnetostriction constant (λ_s) determined by Syono (1965) at 290 and 220 K.

stress (MDS), which is the pressure needed to reduce X_{max} to one-half of its initial value. In many respects, MDS is equivalent to the median destructive field, which is the applied alternating field (AF) needed to destroy one-half of the remanence. This is valid because Néel unblocking curves for AF and stress demagnetization are similar (Dunlop et al., 1969). Figure 12 shows MDS plotted as a function of titanium concentration. Also plotted in Figure 12 are the $1/\lambda_s$ data from Syono (1965) where, to a first order, the relationship between MDS, Ti content and $1/\lambda_s$ is apparent.

An additional problem to address pertains to the decrease in M_s . Comparing reversible susceptibility with the full magnetic vector properties of TM0 suggests that a large portion of M_s must remain at high pressures, and for multidomain grains, the ratio of the remanent saturation moment (M_{rs}) to M_s behaves more like $1/M_s$ (Gilder et al., 2002; 2004). One explanation for the disappearance of M_s might lie in the assumptions behind the reversible susceptibility method, e.g. that X_{rev} is equivalent to X_{diff} for multidomain grains. For example, if stress transforms a certain percentage of X_{rev} into X_{irr} , some of the signal will be lost with the AC susceptibility method. Part of this transformation could occur in multidomain grains in different ways. First, since domains are rotated into the plane perpendicular to the maximum stress direction (Bogdanov and Vlasov, 1966; Appel and Soffel, 1985), domain wall motion would be muted as the AC field direction becomes oriented perpendicular to the domain walls. Second is that the number of dislocations increases with stress, which acts to reduce domain sizes, inhibit wall motion and/or physically create single domain grains or subvolumes that take on single domain properties (Appel and Soffel, 1984). On the other hand, full differential hysteresis loops [$M(H)$] of a titanomagnetite sample also demonstrate a decrease in M_s with pressure (Nagata and Kinoshita, 1964; 1965), and theoretical calculations suggest susceptibility

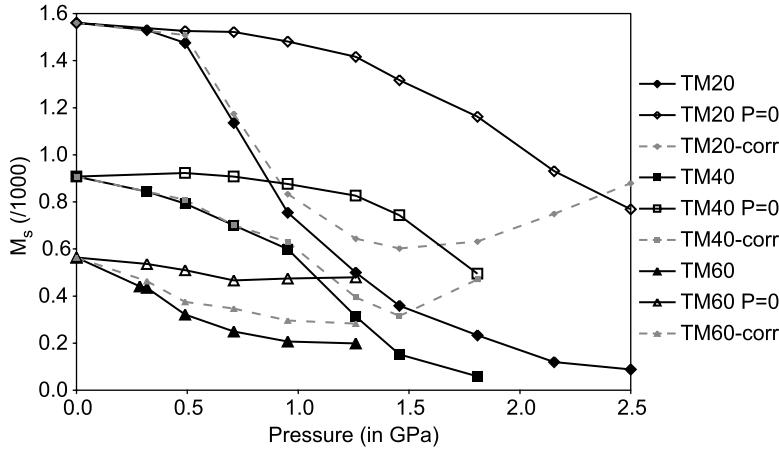


Figure 13. M_s (multiplied by 1/1000) measured in the type-two experiments. Solid symbols are the M_s values measured under pressure (P_n) and the open symbols are the M_s values measured at zero pressure ($P = 0$) after releasing from pressure (P_n). Gray symbols are the M_s values measured under pressure (P_n) corrected by the amount of M_s lost as determined from the zero pressure data. Note that $P = 0$ after $P = P_n$ was not measured for the first pressure step.

varies proportionally with M_s squared (e.g. Stacey, 1962; Nagata, 1966). Thus, it seems that at least part of X_{rev} and M_s must be reduced and not only hidden or transformed into a state dominated by X_{irr} because (1) it has been directly observed and (2) the proportionality between X_{rev} , σ , $1/\lambda_s$ and Ti composition.

The type-two experiments give insight into how much X_{rev} converts to X_{irr} and the bearing that it has on M_s . Figure 13 shows the M_s data for each TM species plotted under pressure (solid symbols) ($P = P_n$) and when pressure was released ($P_n \Rightarrow 0$) from P_n (open symbols). Unfortunately, such data are not available for TM0. M_s at $P_n \Rightarrow 0$ generally decreases as P_n increases, suggesting that the material exhibits less reversibility at higher pressures. If the amount of M_s lost upon pressure release reflects how much X_{rev} is converted to X_{irr} at P_n , then we can add the amount of M_s lost, calculated relative to the initial (starting) value, to M_s measured under the corresponding pressure P_n . Adjusted M_s values are shown in Figure 13 as gray symbols. The adjusted data still decrease with pressure, yet less than before, and there is a tendency for M_s to increase at pressures >1.5 GPa for TM20 and possibly for TM40. Thus, instead of being reduced to $\sim 10\%$ of initial values, they drop only to $\sim 40\%$. Further experimentation should be carried out to understand the changes in M_s .

Comparing M_s with X_{max} can yield additional insight on how stress influences the magnetization process of titanomagnetite. This is done in Figure 14, where the data are plotted from both the type-one and type-two experiments for all pressures. In general, a good correlation exists between TM species, with TM0 having the highest M_s/X_{max} ratios and TM60 the lowest. We suspect that the greater dispersion of the TM20 data arises from the slight contamination with other TM phases (Fig. 6). All four phases exhibit an evolution toward steeper slopes with increasing pressure, until the highest pressures where M_s/X_{max} converges to a constant value (Fig. 14-inset). This could

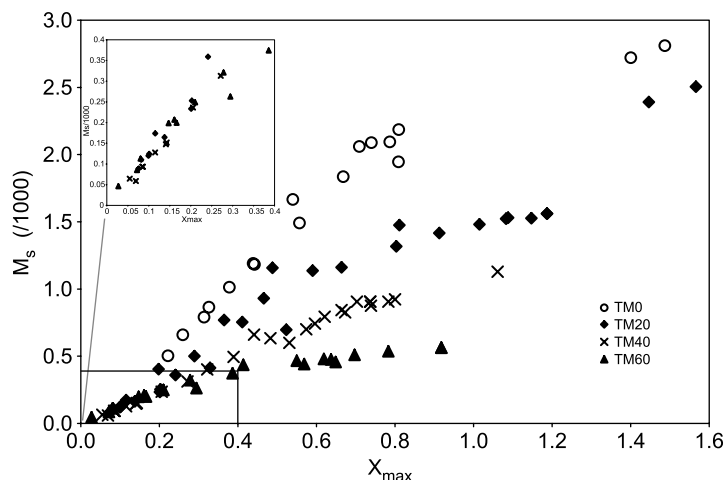


Figure 14. M_s (multiplied by 1/1000) versus X_{\max} for all experiments. M_s/X_{\max} increases with decreasing Ti content. With increasing pressure, M_s/X_{\max} increases for all species except at the highest pressures where M_s becomes proportional to $4/3 X_{\max}$ (inset). Data for TM0 were reported in Gilder et al. (2002).

suggest that the domain production/re-orientation process occurs differently under discrete strain states, e.g. that there are distinct strain regimes until M_s ultimately becomes linearly proportional to N , with all TM phases following the same proportionality law once a given threshold strain state is reached. Systematic changes in the domain configuration brought about by the application of stress was proposed by Kean et al. (1976) to explain differential changes in susceptibility acquired perpendicular or parallel to applied uniaxial stresses.

7. Conclusions

In this chapter we describe the theory behind the AC susceptibility method and the details surrounding the construction of an AC susceptibility system for the diamond anvil cell. By placing the cell within an electromagnet and measuring reversible susceptibility as a function of applied DC field, our system can quantify magnetic hysteresis parameters while being able to detect thermal perturbations or spurious effects from mechanical interactions that potentially occur during an experiment. When a non-electrically conducting substance can be found to serve as a gasket, our system can be adapted to measure the electrical conductivity of material under pressure.

Here, we show that pressure modifies the magnetic properties of titanomagnetite relative to the Ti concentration, with $M_s(P)$ and $X_{\max}(P)$ being inversely proportional to stress and magnetostriction (λ_s). Because λ_s increases with increasing Ti, titanomagnetite species become increasingly pressure sensitive. Thus, by merely knowing the magnetostriction constants of a given magnetic mineral, one should be able to predict its sensitivity to an imposed stress. With this in mind, one can revisit the relevance of piezo-remnant magnetization and stress demagnetization to earthquake prediction or the

build up or relaxation of stress in the crust due to tectonic motion (Stacey, 1964; Davis and Stacey, 1972; Smith and Johnston, 1976; Zlotnicki and Cornet, 1986), which has proved elusive. Terrains containing Ti-rich titanomagnetite phases, such as oceanic crust, should be considered the best targets, while the strain history of the rocks should be accounted for by identifying places where the rocks have been previously subjected to the lowest possible stresses.

Acknowledgements

Special thanks are given to Barbara (B.J.) Wanamaker and Bruce Moskowitz for providing the titanomagnetite. We are grateful for the helpful reviews of Gunther Kletetschka, Özden Özdemir and an anonymous reviewer. Thanks also to Denis Andrault for providing open access to his lab. The diamond cell described in this chapter was designed by Jean-Claude Chervin and his team at the Université Pierre et Marie Curie. This work was funded by INSU (“Intérieur de la Terre” program) and by the IPGP Bonus Qualité de Recherche (IPGP publication #2008).

References

- Adams, D., Appleby, R., Sharma, S., 1976. Spectroscopy at very high pressures: part X. Use of ruby R-lines in the estimation of pressure at ambient and at low temperatures. *J. Phys. E* 9, 1140–1144.
- Akimoto, S., 1962. Magnetic properties of FeO–Fe₂O₃–TiO₂ system as a basis of rock magnetism. *J. Phys. Soc. Jpn* 17 (Suppl. B-1), 706–710.
- Appel, E., Soffel, H.C., 1984. Model for the domain state of Ti-rich titanomagnetites. *Geophys. Res. Lett.* 11, 189–192.
- Appel, E., Soffel, H.C., 1985. Domain state of Ti-rich titanomagnetites deduced from domain structure observations and susceptibility measurements. *J. Geophys.* 56, 121–132.
- Bertotti, G., 1998. *Hysteresis in Magnetism*. Academic Press, San Diego.
- Bogdanov, A.A., Vlasov, A.Ya, 1966. On the effect of elastic stresses on the domain structure of magnetite. *Izv. Phys. Solid Earth* 1, 24–26.
- Chervin, J.C., Canny, B., Besson, J., Pruzan, P., 1995. A diamond cell for IR microspectroscopy. *Rev. Sci. Instrum.* 66, 2595–2598.
- Chervin, J.C., Canny, B., Mancinelli, M., 2001. Ruby-spheres as pressure gauge for optically transparent high pressure cells. *High Pressure Res.* 21, 305–314.
- Davis, P.M., Stacey, F.D., 1972. Geomagnetic anomalies caused by a man-made lake. *Nature* 240, 348–349.
- Dunlop, D.J., 1983. On the demagnetizing energy and demagnetizing factor of a multidomain ferromagnetic cube. *Geophys. Res. Lett.* 10, 79–82.
- Dunlop, D.J., Özdemir, Ö., 1997. *Rock Magnetism*. Cambridge University Press, Cambridge.
- Dunlop, D.J., Ozima, M., Kinoshita, H., 1969. Piezomagnetization of single domain grains: a graphical approach. *J. Geomag. Geoelec.* 21, 513–518.
- Endo, S., Yamada, J., Imada, S., Ishizuka, M., Kindo, K., Miyamoto, S., Ono, F., 1999. Development of magnetization measurement under pressure and pulsed high magnetic field. *Rev. Sci. Instrum.* 70, 2445–2447.
- Eremets, M.I., Struzhkin, V.V., Utjuzh, A.N., 1995. Miniature high pressure cells for high magnetic field applications. *Physica B* 211, 369–371.
- Gilder, S.A., LeGoff, M., Peyronneau, J., Chervin, J.C., 2002. Novel high-pressure magnetic measurements with application to magnetite. *Geophys. Res. Lett.* 29, 10.1029/2001GL014227.

- Gilder, S.A., LeGoff, M., Peyronneau, J., Chervin, J.C., 2004. Magnetic properties of single and multi-domain magnetite under pressures from 0 to 6 GPa. *Geophys. Res. Lett.* 31, L10612, doi:10.1029/2004GL019844.
- Hamano, Y., 1983. Experiments on the stress sensitivity of natural remanent magnetization. *J. Geomag. Geoelec.* 35, 155–172.
- Hodych, J., 1976. Single-domain theory for the reversible effect of small uniaxial stress upon the initial magnetic susceptibility of rock. *Can. J. Earth Sci.* 13, 1186–1200.
- Ishizuka, M., Amaya, K., Endo, S., 1995. Precise magnetization measurements under high pressures in the diamond-anvil cell. *Rev. Sci. Instrum.* 66, 3307–3310.
- Kapicka, A., 1990. Variations of the mean susceptibility of rocks under hydrostatic and non-hydrostatic pressure. *Phys. Earth Planet. Interiors* 63, 78–84.
- Kean, W., Day, R., Fuller, M., Schmidt, V., 1976. The effect of uniaxial compression on the initial susceptibility of rocks as a function of grain size and composition of their constituent titanomagnetites. *J. Geophys. Res.* 81, 861–872.
- Kern, J.W., 1961. The effect of stress on the susceptibility and magnetization of a partially magnetized multidomain system. *J. Geophys. Res.* 66, 3807–3816.
- Kim, C., Reeves, M., Osofsky, M., Skelton, E., Liebenberg, D., 1994. A system for in situ pressure and ac susceptibility measurements using the diamond anvil cell: $T_c(P)$ for $HgBa_2CuO_{4+\delta}$. *Rev. Sci. Instrum.* 65, 992–997.
- Kittel, C., 1949. Physical theory of ferromagnetic domains. *Rev. Mod. Phys.* 21, 541–583.
- Lindsley, D.H., 1991. Oxide Minerals: Petrologic and Magnetic Significance, *Reviews in Mineralogy*, Vol. 25. Mineralogical Society of America, Washington.
- Mao, W.H., Atherton, D.L., 2000. Effect of compressive stress on the reversible and irreversible differential magnetic susceptibility of a steel cube. *J. Mag. Mag. Matter* 214, 69–77.
- Mullins, C.E., Tite, M.S., 1973. Magnetic viscosity, quadrature susceptibility, and frequency dependence of susceptibility in single domain assemblies of magnetite and maghemite. *J. Geophys. Res.* 78, 804–809.
- Nagata, T., 1966. Magnetic susceptibility of compressed rocks. *J. Geomag. Geoelec.* 18, 73–80.
- Nagata, T., Kinoshita, H., 1964. Effect of release of compression on magnetization of rocks and assemblies of magnetic minerals. *Nature* 204, 1183–1184.
- Nagata, T., Kinoshita, H., 1965. Studies on Piezo-magnetization (I) magnetization of titaniferous magnetite under uniaxial compression. *J. Geomag. Geoelec.* 17, 121–135.
- Néel, L., 1955. Some theoretical aspects of rock magnetism. *Adv. Phys.* 4, 191–243.
- O'Reilly, W., 1984. *Rock and Mineral Magnetism*. Chapman & Hall, New York.
- Özdemir, Ö., Xu, S., Dunlop, D., 1995. Closure domains in magnetite. *J. Geophys. Res.* 100, 2193–2209.
- Pozzi, J.P., 1973. *Effets de Pression en Magnétisme des Roches*. Ph.D. Thesis, Université Paris VI, Paris, France.
- Shive, P.N., Butler, R.F., 1969. Stresses and magnetostrictive effects of lamellae in the titanomagnetite and ilmenohematite series. *J. Geomag. Geoelec.* 21, 781–796.
- Smith, B.E., Johnston, M.J.S., 1976. A tectonomagnetic effect observed before a magnitude 5.2 earthquake near Hollister, California. *J. Geophys. Res.* 81, 3556–3560.
- Soffel, H.C., Deutsch, E.R., Appel, E., Eisenach, P., Peterson, N., 1982. The domain structure of synthetic stoichiometric TM10–TM75 and Al-, Mg-, Mn- and V-doped TM62 titanomagnetites. *Phys. Earth Planet. Interiors* 30, 336–346.
- Stacey, F.D., 1962. Theory of the magnetic susceptibility of stressed rock. *Philos. Mag.* 7, 551–556.
- Stacey, F.D., 1964. The seismomagnetic effect. *Pure Appl. Geophys.* 58, 5–22.
- Struzhkin, V.V., Timofeev, Yu., Gregoryanz, E., Mao, H.K., Hemley, R.J., 2002. New methods for investigating superconductivity at very high pressures. In: Hemley, R.J., Bernasconi, M., Ulivi, L., Chiarotti, G. (Eds), *High-Pressure Phenomena, Proceedings of the International School of Physics, "Enrico Fermi" Course CXLVII*. IOS press, Amsterdam, pp. 275–296.
- Syono, Y., 1965. Magnetocrystalline anisotropy and magnetostriction of Fe_3O_4 – Fe_2TiO_4 series with special application to rock magnetism. *Jpn. J. Geophys.* 4, 71–143.
- Timofeev, Y.A., Mao, H.K., Struzhkin, V.V., Hemley, R.J., 1999. Inductive method for investigation of ferromagnetic properties of materials under pressure. *Rev. Sci. Instrum.* 70, 4059–4061.
- Tozer, S.W., 1993. Miniature diamond-anvil cell for electrical transport measurements in high magnetic fields. *Rev. Sci. Instrum.* 64, 2607–2609.

- Valeev, K.A., Absalyamov, S.S., 2000. Remanent magnetization of magnetite under high pressures and shear loads. *Izv. Phys. Solid Earth* 36, 241–245.
- Wanamaker, B.J., Moskowitz, B.M., 1994. Effect of nonstoichiometry on the magnetic and electrical properties of synthetic single crystal $\text{Fe}_{2.4}\text{Ti}_{0.6}\text{O}_4$. *Geophys. Res. Lett.* 21, 983–986.
- Yamamoto, K., Endo, S., Yamagishi, A., Mikami, H., Hori, H., Date, M., 1991. A ceramic-type diamond anvil cell for optical measurements at high pressure in pulsed high magnetic fields. *Rev. Sci. Instrum.* 62, 2988–2995.
- Zlotnicki, J., Cornet, F.H., 1986. A numerical model of earthquake-induced piezomagnetic anomalies. *J. Geophys. Res.* 91, 709–718.

This page is intentionally left blank